# Finite element modelling of wave propagation in highly scattering materials

A. Van Pamel, P. Huthwaite, C. R. Brett, and M. J. S. Lowe

Citation: AIP Conference Proceedings **1706**, 070001 (2016); doi: 10.1063/1.4940519
View online: http://dx.doi.org/10.1063/1.4940519
View Table of Contents: http://scitation.aip.org/content/aip/proceeding/aipcp/1706?ver=pdfcov
Published by the AIP Publishing

# Finite Element Modelling of Wave Propagation in Highly Scattering Materials

A. Van Pamel[1,2], P. Huthwaite[1], C. R. Brett[2], and M. J. S. Lowe[1,a)]

[1]*Department of Mechanical Engineering, Imperial College London, London SW7 2AZ, United Kingdom*
[2]*E.ON Technologies Limited, Technology Centre, Nottingham, NG11 0EE, United Kingdom.*

[a)]m.lowe@imperial.ac.uk

**Abstract.** Ultrasonic inspection of highly scattering materials presents challenges for industry. This article describes a Finite Element modelling methodology to simulate wave propagation within polycrystalline materials. Concerns are answered regarding its required mesh sampling and ability to capture the complex scattering physics. It is shown that grain scattering phenomena are closely reproduced across a range of scattering regimes. The procedure is subsequently applied to investigate the optimal configuration of an array inspecting such a material. It is found that in certain situations, separating emitter and receiver can be advantageous as this reduces the received backscatter.

## INTRODUCTION

The average generation efficiency of current power plants is limited to around 35% for an operation temperature of approximately 565°C. Next-generation ultra-super-critical (USC) power plants [1] aim to increase this temperature to 700°C, thereby enabling efficiencies close to 50+% and reducing specific emissions. This evolution requires sufficiently resilient materials, where Inconel super-alloys have been identified as promising candidates. These materials are prohibitively expensive however [2], and thus the economic feasibility of USC power plants can benefit from NDE to reduce costs.

The very aspect which helps provide the required superior creep strength to enable these temperatures - a coarse polycrystalline microstructure - however also introduces inspection difficulties for ultrasonic NDE. As the wavelength becomes dimensionally similar to that of the grains, scattering occurs, increasing both attenuation and noise which compromise the reliability of inspections.

The ultrasonic inspection of highly scattering materials has received plentiful interest[3], [4] which has led to both experimental studies and the pursuit of modelling tools. One such well-respected model is the Independent Scattering Model[5] which was originally developed in the context of inspections for the aerospace industry. The ISM has proven particularly useful: by predicting the Signal-to-coherent-noise ratio (SNcR) it, for example allows the determination of an optimal inspection configuration or the smallest detectable defect size. The ISM however depends on a single scattering assumption, and hence in order to consider stronger scattering environments, we need to consider different models which are valid within multiple scattering regimes. Amongst the existing approaches, this article adopts an implementation of the Finite Element (FE) method[6]–[8] for simulating ultrasonic wave propagation within polycrystalline materials. The utility of the methodology is demonstrated by investigating an optimal ultrasonic array configuration for the inspection of a future power plant material.

## FINITE ELEMENT MODELLING OF POLYCRYSTALS

### Methodology

The FE approach adopts an established Voronoi[6]–[8] approach which enables randomly generating, in this case, relatively simple polycrystalline microstructures: single phased, untextered, and equiaxed materials. The procedure requires an input random spatial distribution of points, which using the Voronoi algorithm produces a random tessellation, such that each original point becomes the seed for a grain. Once a grain morphology is generated, it

*42nd Annual Review of Progress in Quantitative Nondestructive Evaluation*
AIP Conf. Proc. 1706, 070001-1–070001-9; doi: 10.1063/1.4940519

requires regularization[9] before meshing the model as prescribed by FE. Finally, each grain is assigned a random crystallographic orientation (to create an untextered material) to define the acoustic impedance mismatch which brings rise to scattering.

Due to the relatively recent emergence of this modelling approach, several questions still remain regarding its implementation. One such question concerns the mesh requirements which determines the computational efficiency and accuracy of the solutions. Several possibilities exist here, one is to opt for a mesh which uses arbitrary shapes such that it conforms to the grain boundaries, known as an unstructured mesh (see Figure 1a), and another is to approximate the grains by regularly shaped structured meshes (see Figure 1b).

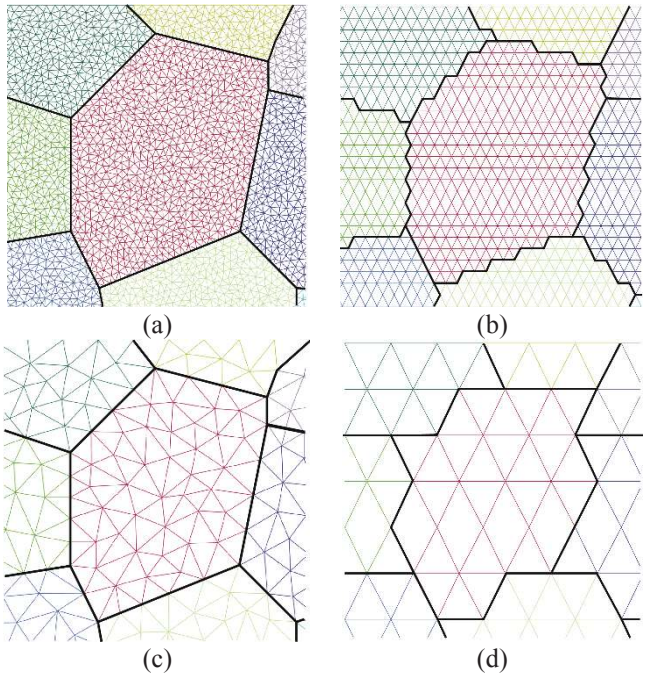


**FIGURE 1.** Typical grain meshed using a fine (a) unstructured and (b) structured mesh. The coarse mesh equivalent is shown for a (c) unstructured, and (d) structured mesh.

## Mesh Convergence Study

The mesh performance is assessed by monitoring both the error in amplitude and time-of-flight (TOF) for a plane wave propagating within a 2D slab of polycrystalline material (see Figure 2), whilst varying the mesh density. (An example of a fine and a coarse mesh is provided in Figure 1 for both types of mesh.) The plane wave is excited using an approach similar to that used by Choi[10], which uses symmetry boundary conditions at the horizontal-edges of the slab (the lines where y=0 and y=12mm in Figure 2), and applies a force load (in this case a 2MHz 3 cycle toneburst) to the nodes along the vertical-edge where x=0mm. The receiving signal is recorded by averaging the nodal displacement along the entire width of the slab at the opposite end of the excitation source (the line where x=42mm). Two different meshes are investigated, both a structured, and unstructured mesh employing triangular element shapes, each for three different grain size distributions, defined by a mean grain size of 100 μm, 250 μm, and 500μm.
The result in Figure 3 shows the convergence of error metrics for the group velocity (calculated from TOF) and the amplitude as the mesh is refined. As can be observed, both metrics converge to within 1% at around 10 elements per grain. This demonstrates that the grains introduce a new meshing criterion, in addition to the conventional sampling (10 elements per wavelength) criterion[11], which in this particular case proved to be stricter.

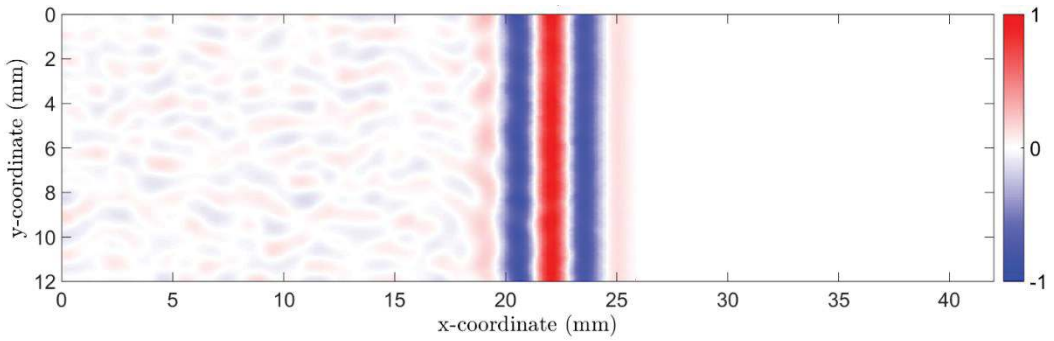


**FIGURE 2.** Plane wave propagating within a 2D slab of polycrystalline material after 4.5 μs.

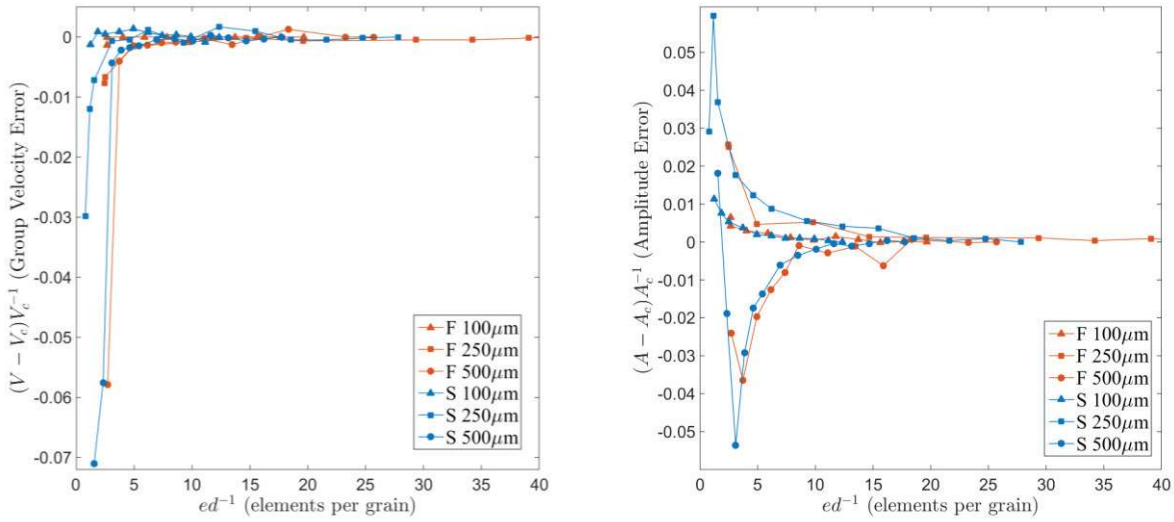


(a) (b)

**FIGURE 3.** Convergence of (a) group velocity (b) amplitude error versus mesh density.

## Validation

Now that convergence has been achieved, the next question concerns the capability of FE to recreate grain scattering phenomena. This is not trivial given the complex grain scattering behavior which manifests three regimes depending on the wavelength to grain size ratio. Within the long wavelength regime there is a fourth order frequency dependence of attenuation, known as Rayleigh scattering. At higher frequencies, once the wavelength approaches and reduces below the grain size, the scattering mechanism converges to a second order dependence, known as a stochastic regime. Eventually, at even higher frequencies, attenuation becomes independent of frequency in the geometric regime. This is illustrated in Figure 4a (see black-line only) which plots the normalized attenuation, such that it is independent of grain size, against the normalized frequency, as defined by the Unified Theory[12] for the material properties of Inconel 600[7].

The FE model consists of both 2D models with a mean grain size of 500μm and 100μm, and a 3D model with a mean grain size of 500μm. Each are excited, similarly to the previous section, to propagate plane waves exhibiting center frequencies between 1-4MHz.

The raw results are shown in Figure 4b-d. At first glance, the attenuation is shown to increase with frequency, which is promising first step. However, in comparison to anticipated fourth power coefficient found for the 3D simulations, it can be seen that 2D scattering fails to recreate the same frequency dependence, as it is instead reduced to a third order dependence. The reduction of this power coefficient within the Rayleigh scattering is thought to be a consequence of the simplifying dimensions used in 2D, although we provide no proof here.

The results in Figure 4b-d are replotted against the Unified Theory in Figure 4a, on a log-log plot, with normalized frequency on the x-axis, and normalized attenuation (as mentioned previously) on the y-axis. The comparison reveals that the FE model closely predicts the correct attenuation trends, even across different regimes which embody various scattering mechanisms.

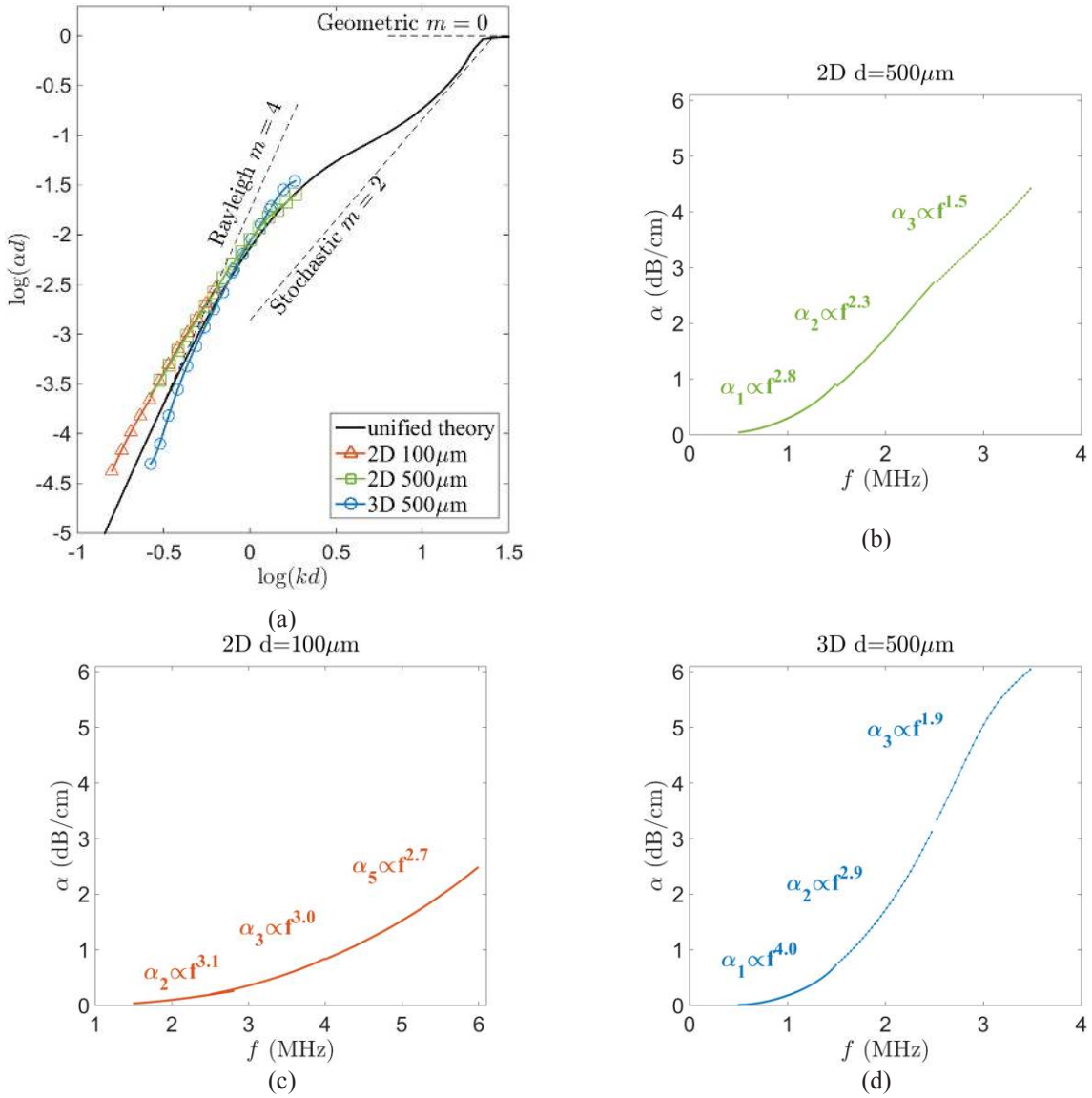


**FIGURE 4.** Attenuation versus frequency results for (a) the Unified Theory [12] (b) 2D material and 500μm grain size (c) 2D material and 100μm grain size (d) 3D material and 500μm grain size. The results of (b) to (d) are also superposed in (a) to allow comparison with the Unified Theory.

## ARRAY CASE STUDY

The modelling methodology outlined above is used to demonstrate its utility by way of a practical example. We adopt arrays as our case of interest as they present promising[13] opportunities for improving ultrasonic NDE of noisy materials. Through these simulations, we aim to shed new light onto their optimal configuration. This will be achieved here by setting out to measure the ScNR of the different transmit and receive combinations of the array. This requires both a signal and noise model which are discussed next.

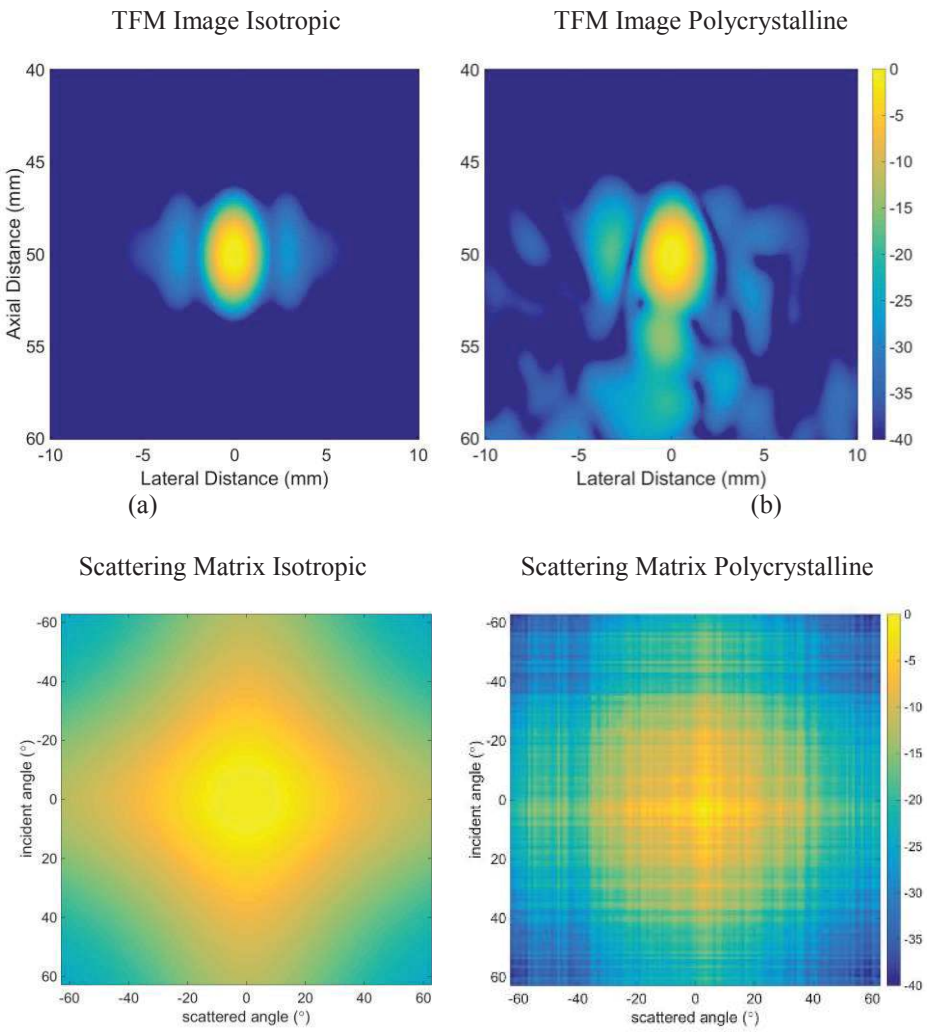


**FIGURE 5.** TFM image of a true point scatterer with (a) isotropic and (b) polycrystalline medium. The scattering matrix for a true point scatterer with a (c) isotropic and (d) polycrystalline medium.

## Simulation

The model layout comprises a 128 element array with a 2MHz center frequency in a contact configuration with an elastic medium. This simulation is repeated for both an arbitrary isotropic material and a polycrystalline material. The former is defined such that it has similar macro properties to the latter: Inconel 600 (properties taken from [7]) with a mean grain size of 500μm. Whereas plane waves were used previously, the array is simulated by firing the half-wavelength sized array elements sequentially, by applying a pressure load on the surface of the sample which corresponds to their footprint, and recording the received signals across all the array elements, for each sequence. This populates a data matrix known as the Full Matrix Capture (FMC)[14].

### *Signal Model*

For the signal model, which involves acquiring the FMC containing the signal data, denoted by $FMC_s$, we simulate a True Point Source (TPS). Whereas usually the array element are fired (as described above), here the defect is illuminated to create a circular point source and the resulting signals are received across all the array elements. Using a reciprocity argument this can be exploited to obtain an $FMC_s$ which reproduces the FMC of the defect response

minus the backscatter which would otherwise be present when using a conventional FMC firing sequence. Such an omnidirectional scatterer offers a desirable benchmark as it allows us to investigate the fundamental performance of the array without including other dependencies such as the anisotropic scattering behavior of most defects.

Once the signal $FMC_S$ is obtained the resulting Total Focusing Method (TFM) images are calculated. This is shown in Figure 5a-b for the simulation results of an isotropic and a polycrystalline medium. This isotropic simulation confirms that the TPS behaves as desired and also provides a comparison to the polycrystalline solution.

Aside from the TFM images, we can derive additional information from these results by also plotting an apparent scattering matrix[15]. Namely, by calculating the scattering amplitude as a function of scattering and received angle (according to the transmitted and received array element combination), we can observe the scattering behavior of the defects. The equivalent matrix for the isotropic medium is shown in Figure 5c and again confirms the anticipated behavior of an omnidirectional scatterer. Any decrease in amplitude for angles away from (0°,0°), are due to the longer propagation distances (beam spreading) and a loss in element sensitivity (directivity). The scattering matrix for the equivalent TPS within a polycrystalline medium (see Figure 5d) shows that aberrations have occurred in the peak signal for the polycrystalline medium. On average however, the TPS maintains behavior similar to an isotropic scatterer.

### *Noise Model*

The noise model follows the conventional sequential firing sequence as described previously to produce an FMC. This is labelled as an $FMC_N$, as without the introduction of a defect within the material, this provides a measurement pertaining solely to the background scattering noise. Although artificial in this case, this is similar to what is referred to as a baseline in structural-health-monitoring[16].

The same post-processing procedure to calculate an apparent scattering matrix as outlined above for the signal model, is repeated using the $FMC_N$ data as its input. This produces a noise scattering matrix, plotted here in Figure 6a, and it reveals several interesting behaviors. Firstly, along the leading diagonal, which corresponds to the pulse-echo combinations of the array, there is a notable increase in the backscattered amplitude. This is due to reciprocity which doubles the amount of noise received for pulse-echo elements, as any scattering path which originates from an array element and leads back to it, will also exist in the reverse order (whereas this is not the case for the pitch-catch combinations see e.g Shahjahan[7]). This also explains why twin-crystal probes are often preferable when inspecting highly scattering materials.

The second observation to note is the existence of a large region which contains significantly higher noise. This is defined here as the backscatter envelope, and operating outside it offers an opportunity to receive a longitudinal wave before the majority of backscatter has arrived. At the limit of the backscatter envelope, there is a sudden increase in the noise amplitude, recognizable as quarter-circle bands, which quickly drops again. This peak is found to correspond to the Rayleigh wave and thus defines the limit of the backscatter envelope. In order to illustrate and clarify the significance of this concept, we will demonstrate it experimentally.

## Experiment

The basis of this experiment is to acquire an ultrasonic array image with a single array, which operates well within the backscatter envelope, and compare it to the equivalent image acquired with a dual array setup (see Figure7a). The dual array physically separates the arrays (in this case by 25mm) such that an opportunity exists to receive backwall signals before the majority of backscatter has arrived. The inspected material consists of a copper block and the array setup (LECOUER, France) uses two identical arrays with 64 elements and a 5MHz center frequency (IMASONIC, France). In order to ensure electrical noise is suppressed, sufficient temporal averaging is applied to each FMC acquisition such that the noise floor is defined by coherent noise only.

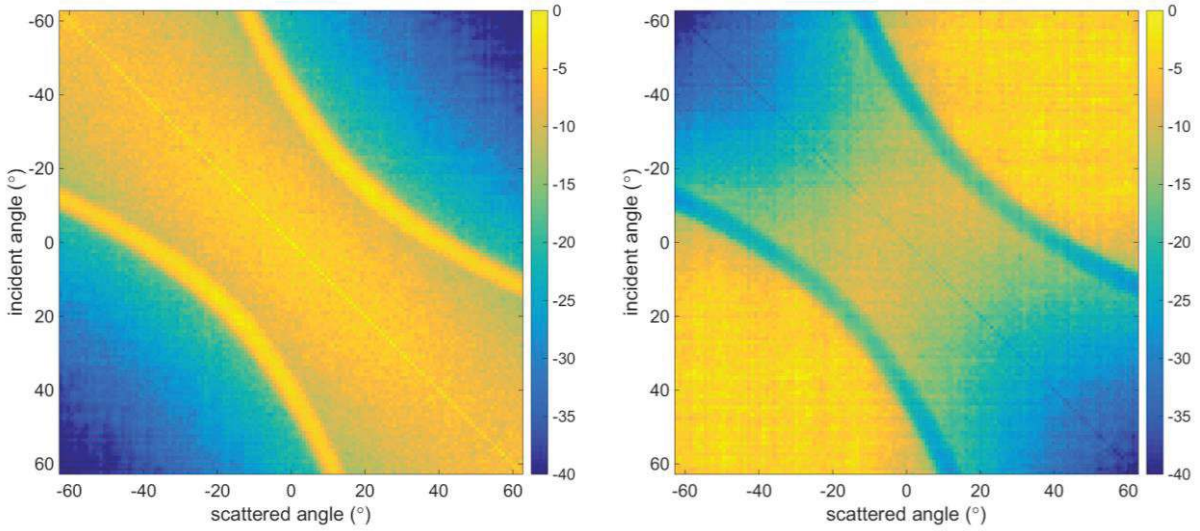


(a) (b)

**FIGURE 6.** (a) Noise Scattering Matrix, and (b) the SNR matrix.

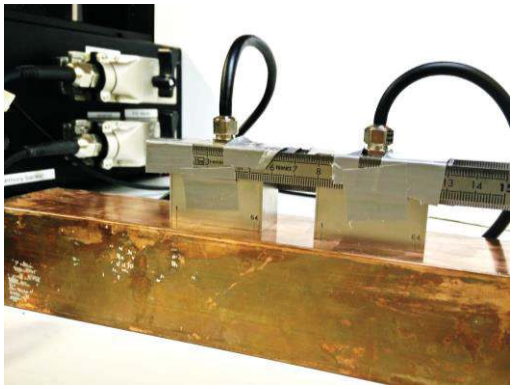

(a)

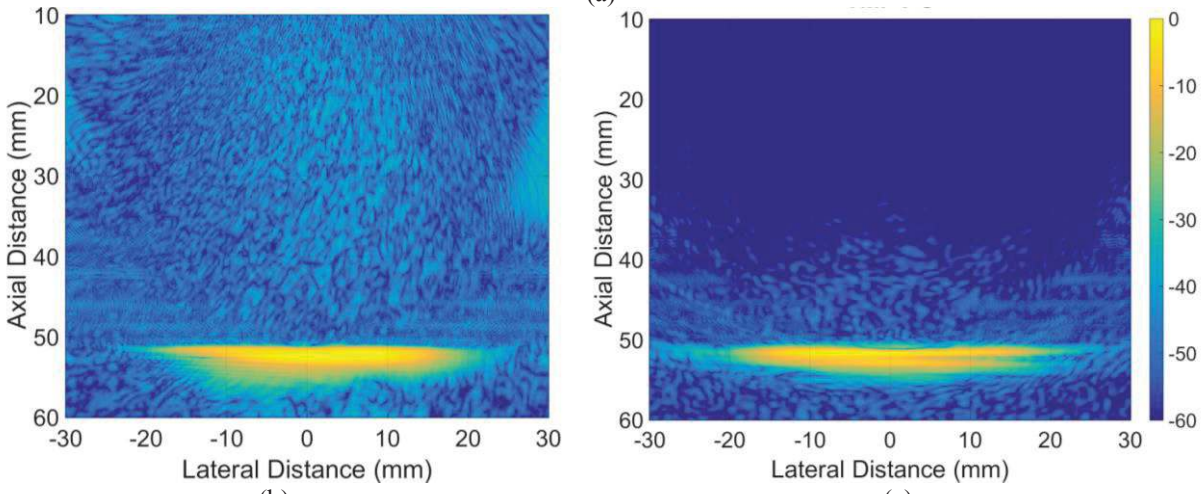


(b) (c)

**FIGURE 7.** (a) Experimental setup of two arrays separated by 25mm in contact with copper. TFM images of the back wall for the (b) single array and (c) dual array setup.

Figure 7b plots the resultant TFM image for a single array and reveals that the backwall is detected with ScNR of 50dB. The TFM image of a dual array (Figure 7c) conversely shows that the ScNR has improved by 8dB due to a reduction in the received backscatter. This result is in agreement with the previous simulations and demonstrates that separating source and emitter can create an advantage to outrun the backscatter envelope with a longitudinal wave which corresponds to a feature of interest. The authors would like to emphasize that such an opportunity will not exist for all practical scenarios, we merely aim to illustrate and explain this effect which was previously only observed empirically. This demonstrates the utility of the FE modelling methodology to study such phenomena.

## CONCLUSION

This article has discussed a Finite Element methodology for the simulation of elastic wave scattering within polycrystalline materials. The requirements for mesh convergence for both a structured and unstructured mesh were discussed. Furthermore, its capability to simulate scattering phenomena was established through comparisons of attenuation results against established theory. This revealed that FE captures the complex scattering physics across a range of scattering regimes. In order to illustrate the benefits of the model, the second part of the article adopted the aforementioned modelling approach and applied it to investigate an optimal configuration for an array inspecting a highly scattering material. It was found that in certain situations, separating emitter and receiver array can be advantageous as this allows operation outside the backscatter envelope.

## ACKNOWLEDGMENTS

The authors are grateful to Professor Peter Nagy from the University of Cincinnati for helpful discussions. This work has been supported by the UK Research Centre in NDE and the Engineering and Physical Sciences Research Council grant EP/I017704/1.

## REFERENCES

1. J. Bugge, S. Kjær, and R. Blum, “High-efficiency coal-fired power plants development and perspectives,” Energy, vol. 31, no. 10–11, pp. 1437–1445, 2006.
2. J. Phillips and M. Wheeldon, “Economic Analysis of Advanced Ultra-Supercritical Pulverized Coal Power Plants: A Cost-Effective CO2 Emission Reduction Option?” in Advances in Materials Technology for Fossil Power Plants Proceedings from the Sixth International Conference (ASM International), pp. 53–65, (2011).
3. R. B. Thompson, F. J. Margetan, P. Haldipur, L. Yu, a. Li, P. Panetta, and H. Wasan, “Scattering of elastic waves in simple and complex polycrystals,” Wave Motion, vol. 45, no. 5, pp. 655–674, 2008.
4. F. Margetan, T. Gray, and R. Thompson, “A technique for quantitatively measuring microstructurally induced ultrasonic noise,” in Review of Progress in Quantitative Nondestructive Evaluation, eds. D. E. Chimenti and D.O. Thompson, (Plenum Press, NY), vol 10B, pp.1721 -1728 (1991).
5. F. J. Margetan, R. B. Thompson, and I. Yalda-Mooshabad, “Backscattered microstructural noise in ultrasonic toneburst inspections,” J. Nondestruct. Eval., vol. 13, no. 3, pp. 111–136, Sep. 1994.
6. B. Chassignole, V. Duwig, M.-A. Ploix, P. Guy, and R. El Guerjouma, “Modelling the attenuation in the ATHENA finite elements code for the ultrasonic testing of austenitic stainless steel welds,” Ultrasonics, vol. 49, no. 8, pp. 653–8, 2009.
7. S. Shahjahan, F. Rupin, A. Aubry, B. Chassignole, T. Fouquet, and A. Derode, “Comparison between experimental and 2-D numerical studies of multiple scattering in Inconel600 by means of array probes.,” Ultrasonics, vol. 54, no. 1, pp. 358–67, 2014.
8. G. Ghoshal and J. a. Turner, “Numerical model of longitudinal wave scattering in polycrystals,” IEEE Trans. Ultrason. Ferroelectr. Freq. Control, vol. 56, no. 7, pp. 1419–1428, 2009.
9. R. Quey, P. R. Dawson, and F. Barbe, “Large-scale 3D random polycrystals for the finite element method: Generation, meshing and remeshing,” Comput. Methods Appl. Mech. Eng., vol. 200, no. 17–20, pp. 1729–1745, 2011.

10. W. Choi and E. Skelton, "Unit cell finite element modelling for ultrasonic scattering from periodic surfaces," in Review of Progress in Quantitative Nondestructive Evaluation, eds. D. E. Chimenti and D.O. Thompson, (American Institute of Physics 1511, Melville NY) vol 32, pp. 83-90, (2013).
11. M. B. Drozdz, "Efficient Finite Element Modelling of Ultrasound Waves in Elastic Media," Imp. Coll. London Mech. Eng. PhD Thesis, 2008.
12. F. E. Stanke, "A unified theory for elastic wave propagation in polycrystalline materials," J. Acoust. Soc. Am., vol. 75, no. 3, p. 665, 1984.
13. P. D. Wilcox, "Array imaging of noisy materials," in Review of Progress in Quantitative Nondestructive Evaluation, eds. D. E. Chimenti and D.O. Thompson, (American Institute of Physics 1335, Melville NY) vol 30, pp. 890–897 (2011).
14. C. Holmes, B. W. Drinkwater, and P. D. Wilcox, "Post-processing of the full matrix of ultrasonic transmit – receive array data for non-destructive evaluation," NDT E Int., vol. 38, pp. 701–711, 2005.
15. P. D. Wilcox and A. Velichko, "Efficient frequency-domain finite element modeling of two-dimensional elastodynamic scattering," J. Acoust. Soc. Am., vol. 127, no. 1, pp. 155–65, 2010.
16. A. J. Croxford, P. D. Wilcox, B. W. Drinkwater, and G. Konstantinidis, "Strategies for guided-wave structural health monitoring," Proc. R. Soc. A Math. Phys. Eng. Sci., vol. 463, no. 2087, pp. 2961–2981, 2007.